The Astronomical Journal, 124:2790–2798, 2002 November

3.4 MICRON FEATURE ON THE SHOULDER OF ICE-BAND ABSORPTIONS IN THREE LUMINOUS YOUNG STELLAR OBJECTS: IRAS 18511+0146, IRAS 21413+5442, AND IRAS 04579+4703

Miki Ishii[1] and Tetsuya Nagata
Department of Astrophysics, Nagoya University, Furo-cho, Chikusa-ku, Nagoya 464-8602, Japan

Antonio Chrysostomou[2]
Joint Astronomy Centre, 660 North A'ohoku Place, University Park, Hilo, HI 96720

and

James H. Hough
University of Hertfordshire, Hatfield, Hertfordshire AL10 9AB, UK
Received 2002 April 1; accepted 2002 August 6

ABSTRACT

An absorption feature at 3.4 μm has been detected in the long-wavelength wing of the 3.1 μm H_2O ice feature in three young stellar objects: IRAS 18511+0146, IRAS 21413+5442, and IRAS 04579+4703. The profile of the 3.4 μm absorption in IRAS 18511+0146 has distinct subfeatures at 3.38, 3.41, and 3.48 μm and is not similar to those found in molecular clouds but is similar to those in the diffuse interstellar medium, such as the lines of sight toward the Galactic center and Cyg OB2 12. Spectropolarimetry of the 3.4 μm feature in IRAS 18511+0146 shows no excess polarization accompanying the feature, which is consistent with the observation toward the Galactic center source IRS 7 by Adamson et al.The 3.4 μm absorption in IRAS 18511+0146 probably occurs in the diffuse interstellar medium intervening in the line of sight to the molecular cloud where the H_2O ice absorption occurs. Furthermore, the 3.4 μm absorption carrier seems to reside in a population of nonpolarizing grains in the diffuse interstellar medium, physically separate from other polarizing grains.

Key words: circumstellar matter — dust, extinction — infrared radiation — ISM: lines and bands — stars: pre–main-sequence

1. INTRODUCTION

Although it is generally believed that silicates and some form of carbon dominate interstellar dust, the composition of carbon-rich dust is still very uncertain. Carbon-rich dust has been identified by means of the absorption at 3.4 μm first detected in the sight line to the Galactic center (Soifer, Russell, & Merrill 1976). The absorption is attributed to —CH_2— and —CH_3 groups in aliphatic hydrocarbons (Sandford et al. 1991) and has been observed in a few other sources whose extinction is due to dust in the diffuse interstellar medium (DISM; Sandford, Pendleton, & Allamandola 1995; Pendleton et al. 1994; Imanishi et al. 1996). However, the aliphatic hydrocarbon feature at 3.4 μm has not been unambiguously detected in molecular cloud sources (Allamandola, Sandford, & Tielens 1992, 1993). Instead, dust in molecular clouds shows broad 3.3–3.6 μm absorption on the long-wavelength edge of the 3.1 μm H_2O ice-band absorption. This "long-wavelength wing" might be due to some sort of hydrocarbon (Smith, Sellgren, & Tokunaga 1989) but is unlikely to be caused by such aliphatic hydrocarbons as those in the DISM (Smith, Sellgren, & Brooke 1993). In addition, an absorption feature at 3.47 μm superposed on the long-wavelength wing has been found in several young stellar objects (YSOs) embedded in molecular clouds (Sellgren, Smith, & Brooke 1994; Brooke, Sellgren, & Smith 1996; Brooke, Sellgren, & Geballe 1999; Allamandola et al. 1992).

This feature is identified as C−H stretching vibrations in tertiary carbon atoms (interstellar "diamonds") by Allamandola et al. (1992). Thus, the —CH_2— and —CH_3 bands at 3.4 μm appear to be absent in the lines of sight through molecular clouds, and this implies that carbon-rich materials in the DISM might not survive incorporation into molecular clouds (Allamandola et al. 1993; Tielens et al. 1996).

Recently, a sample of luminous embedded YSOs was observed with low-resolution spectroscopy ($R \sim 40$) from 1.3 to 4.2 μm, and H_2O ice absorption was detected in several objects (Ishii et al. 1998). Among them, three objects—IRAS 04579+4703, IRAS 18511+0146, and IRAS 21413+5442 (hereafter IRAS 04579, IRAS 18511, and IRAS 21413, respectively)—showed the 3 μm absorptions whose profiles were different from those observed previously in YSOs (e.g., Smith et al. 1989); a shallow absorption is seen at 3.4 μm overlying the slope of the broad wing. In addition, the 3.4 μm absorption in IRAS 18511 was clearly confirmed in spectra obtained with higher resolution ($R \sim 250$). The 3.4 μm absorption in the three objects appeared to be different in peak wavelength and width from the 3.47 μm absorption in molecular clouds and rather reminiscent of the 3.4 μm absorption in diffuse clouds. If the 3.4 μm feature of these objects originates in molecular clouds where the H_2O ice absorption occurs, this is the first quantified example of the coexistence of both features. However, the low-resolution spectra taken by Ishii et al. (1998) were insufficient to make a detailed comparison with the profiles observed in diffuse clouds.

In this paper, we report observations with higher resolution ($R \sim 1400$) to investigate the nature of the 3.4 μm

[1] Visiting Astronomer, United Kingdom Infrared Telescope.
[2] Present address: University of Hertfordshire, Hatfield, Hertfordshire AL10 9AB, UK.

absorption in the three objects. Spectropolarimetry was also performed for IRAS 18511, which has an optical depth in the 3.4 μm feature that is one of the largest found outside the Galactic center region (see Sandford et al. 1995; Imanishi et al. 1996). The observations and the results are described in § 2. The spectral features of individual objects are described and possible locations where this absorption occurs are discussed in § 3.

2. OBSERVATIONS AND DATA REDUCTION

2.1. *Spectroscopy*

The 2.87–4.06 μm spectra of IRAS 18511 and IRAS 21413 and the 2.87–3.50 μm spectrum of IRAS 04579 were obtained with the facility infrared Cooled Grating Spectrometer 4 (CGS4) at the United Kingdom Infrared Telescope (UKIRT) on Mauna Kea on 1998 August 6. Weather conditions were good throughout. CGS4 employed a 256×256 InSb array with each pixel corresponding to $0''.61$, a 40 line mm^{-1} grating, and a 1 pixel wide slit. The spectral resolution was 0.0025 μm, and the wavelength coverage for one grating position was 0.64 μm. The spectra were sampled every $\frac{1}{3}$ of a resolution element. For background subtraction, the telescope was nodded about $7''$ along the slit, which was oriented north-south on the sky. A log of the observations is presented in Table 1.

All data were reduced with IRAF.[3] Each frame was bias-subtracted and flat-fielded. The flat-field frame was taken at each grating position by observing a blackbody source internal to CGS4. Background emission was removed by subtracting the nodded frame. Wavelength calibration was obtained from an argon lamp and is accurate to less than 0.001 μm. Then individual spectra were extracted and combined to produce a final spectrum. Spectra of objects were further divided by those of standard stars with spectral types of A–B to remove atmospheric features. The differences in air mass between the objects and the standard stars were within 0.1, or 0.2 in the case of the shorter wavelength observations of IRAS 21413 and IRAS 04579. The standard stars were also used for flux calibration, assuming a blackbody spectrum with a temperature derived from their spectral types. The blackbody functions were normalized to the flux at L. The L magnitudes were taken from the infrared catalog of Gezari et al. (1993), and those not in the catalog were derived from the V magnitudes assuming the $V-L$ colors of their spectral types (Tokunaga 2000). The standard stars are given in column (4) of Table 1 along with their spectral types (col. [5]), the assumed blackbody temperatures (col. [6]), and the L magnitudes (col. [7]). The error in the flux level was estimated to be about 15%. For IRAS 18511 and IRAS 21413, whose spectra were taken at two grating positions, the spectra at the shorter wavelengths were scaled to those at the longer ones. The scaling factors are 0.97 for both of them. The resulting spectra are shown in Figure 1 as solid lines.

Since we did not remove hydrogen absorption lines in the standard stars, division by the standards results in apparent H I emission lines, which are present at 3.04 μm (Pfϵ), 3.30 μm (Pfδ), 3.69 μm (Hu18), 3.74 μm (Pfγ), 3.82 μm (Hu16), 3.91 μm (Hu15), 4.02 μm (Hu14), and 4.05 μm (Brα). On the other hand, it is very likely that these emissions are due in part to intrinsic features in the objects, and we actually confirmed the presence of Brα and Pfγ emissions for IRAS 21413 and Brα emission for IRAS 18511 in the spectra before the division by the standards. For IRAS 04579, sharp and deep atmospheric absorptions in the 3–3.4 μm region prevent us from detecting any stellar features in the spectrum without the division by the standard star. However, it is possible that part of the Pfϵ and Pfδ emission in IRAS 04579 is intrinsic, because the object has Brγ emission in its K band spectrum (Ishii et al. 2001).[4]

We compared the reduced spectra with the low-resolution spectra ($\lambda/\Delta\lambda \sim 40$) taken with the Prism Array Spectrophoto/Polarimeter 2 (PASP2; Ishii et al. 1998) to check the consistency between the two data. In Figure 1, the PASP2 data (*open circles*) are scaled to the CGS4 data (*solid lines*) with factors of 0.94, 0.84, and 2.6 for IRAS 18511, IRAS 21413, and IRAS 04579, respectively. It is plausible that the flux levels obtained with PASP2 for IRAS 18511 and IRAS 21413 are higher than those with CGS4, because PASP2 used a larger aperture ($2''.5$ radius) than CGS4 and these objects are accompanied by nebulosity in the near-infrared (NIR; Ishii et al. 2002). For IRAS 04579, however, the flux level with CGS4 is much higher than that with PASP2, even taking into account an error of 10% for CGS4 and ~15% for PASP2. Thus, the object may be variable. On the other hand, the scaled spectral energy distributions (SEDs) obtained with PASP2 agree very well with the CGS4 data.

[3] IRAF is distributed by the National Optical Astronomy Observatory, which is operated by the Association of Universities for Research in Astronomy, Inc., under cooperative agreement with the National Science Foundation.

[4] The object also shows the H_2 2–1 O(3) emission at 2.97 μm in the CGS4 spectrum.

TABLE 1

Log of the Spectroscopic Observations

Object	Range (μm)	t[a] (s)	Standard	Spectral Type[b]	T_{BB}[c] (K)	L[d] (mag)
IRAS 18511+0146	2.87–3.50	240	BS 7236	A0 IV	9480	3.62
	3.43–4.06	240	BS 7236	A0 IV	9480	3.62
IRAS 21413+5442	2.87–3.50	880	BS 8335	B2.5 III	19000	4.8
	3.43–4.06	160	BS 8335	B2.5 III	19000	4.8
IRAS 04579+4703	2.87–3.50	360	BS 1641	B3 V	19000	3.68

[a] Exposure time.
[b] Spectral type of the standard stars.
[c] Assumed blackbody temperature of the standard stars.
[d] L magnitude of the standard stars.

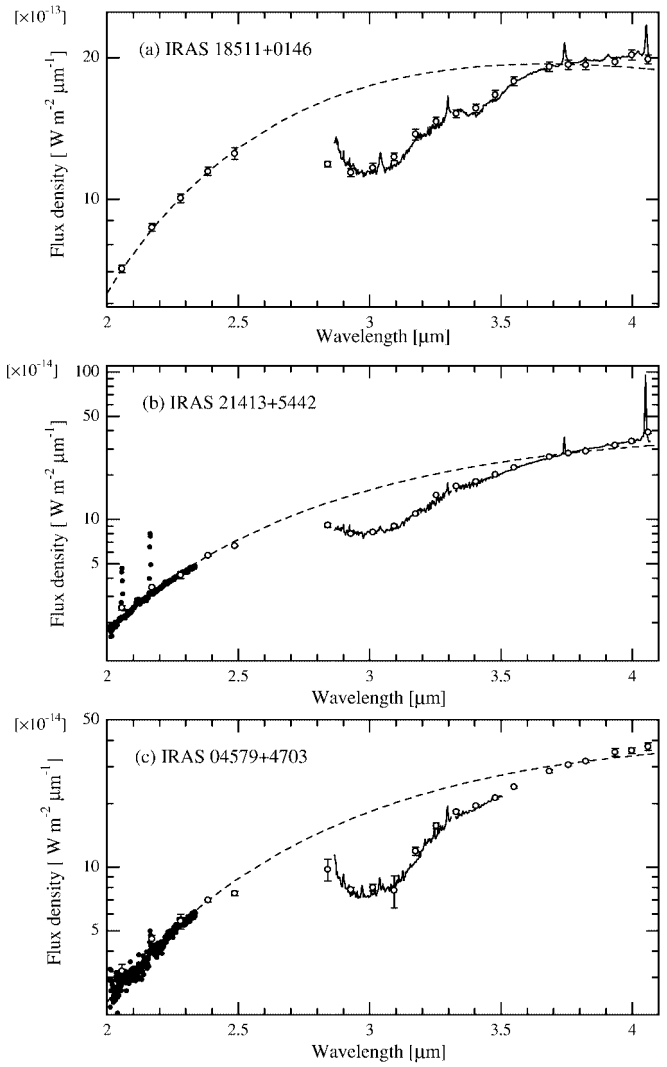

FIG. 1.—2–4 μm spectra of the observed objects. Solid lines starting from 2.9 μm are our observations. Open circles and filled circles represent the 1.3–4.2 μm spectra ($R \sim 40$) by Ishii et al. (1998) and 2–2.33 μm spectra ($R \sim 500$) by Ishii et al. (2001), respectively; these data are scaled to the same flux level as our observations. Dashed lines are blackbodies with temperatures of 790, 570, and 590 K for IRAS 18511, IRAS 21413, and IRAS 04579, respectively.

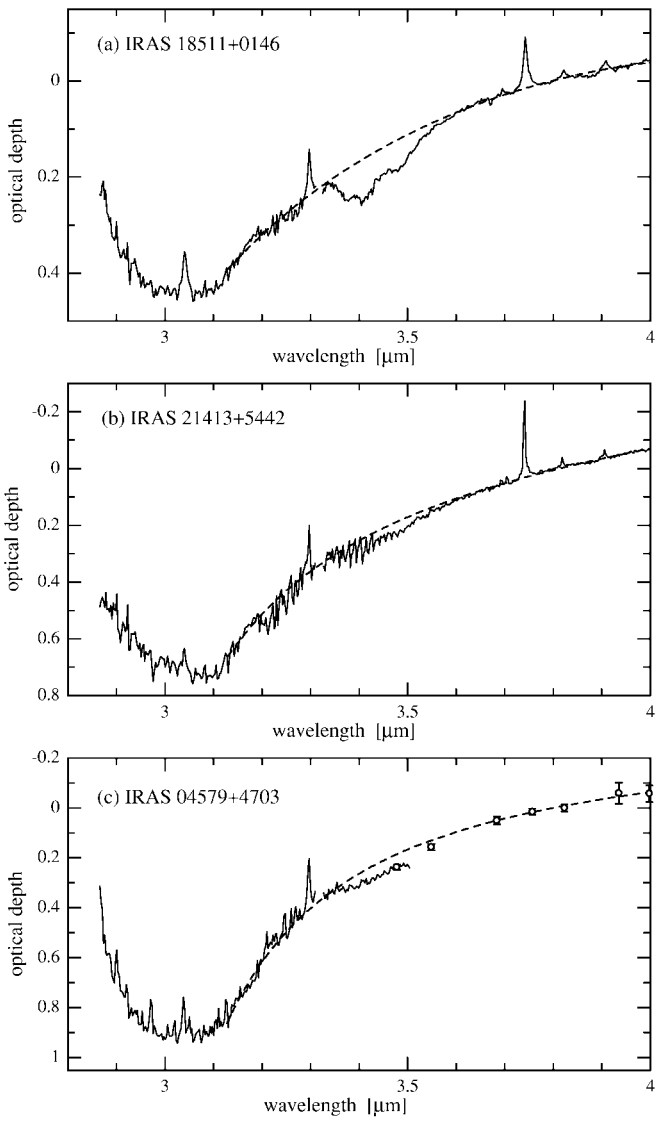

FIG. 2.—Optical depths of the 3 μm ice band absorption (*solid lines*). Dashed lines represent the local continua for the 3.4 μm absorptions, derived by fitting a polynomial function to the observed flux densities at 3.13–3.18, 3.33–3.34, and 3.61–4.00 μm.

We estimate the continuum emission above the ice-band absorption by using a blackbody function. Since the wavelength coverage of our observations was not sufficient for determining the continuum above the 3 μm absorptions, blackbody fitting was applied to the data taken with PASP2, and the points at 2.4 and 3.8 μm were used.[5] The continua are shown in Figure 1 as dashed lines. The blackbody temperatures are 790, 570, and 590 K for IRAS 18511, IRAS 21413, and IRAS 04579, respectively. The optical depths relative to the continua are shown in Figure 2 as solid lines.

[5] Although Ishii et al. (1998) also used a blackbody to estimate the continuum above the 3 μm absorptions, the wavelengths of the fitted points are shorter (2.2 and 3.8 μm). This resulted in blackbody temperatures $\sim$10 K higher than ours for IRAS 21413 and IRAS 04579, and the optical depths changed $\lesssim$0.1. However, profiles of the H_2O feature do not change significantly.

The peak optical depth ($\tau_{\max}$), FWHM ($\Delta\nu$ cm^{-1}), and column density of the H_2O ice feature [$N(H_2O)$] are listed in Table 2; $N(H_2O)$ was calculated from the relation

$$N(\mathrm{H_2O}) \cong \frac{\tau_{\max}\Delta\nu}{A} \ , \qquad (1)$$

where A, the integrated band absorbance, is 2.0×10^{-16} cm molecule^{-1} (d'Hendecourt & Allamandola 1986).

To obtain the 3.4 μm absorption on the long-wavelength wing of the H_2O ice band, we defined the local continuum to be represented by data points in the ranges 3.13–3.18, 3.33–3.34, and 3.61–4.00 μm (except for the points near H I lines: 3.74, 3.82, and 3.92 μm). The continuum is almost the same as that used by Brooke et al. (1999), which was defined to extract the absorptions at 3.47 and 3.25 μm in molecular clouds, with the exception that we avoid the range between 3.34 and 3.37 μm, where the 3.4 μm absorption in diffuse clouds falls. For IRAS 04579, since our observation did not cover the wavelengths longer than 3.5 μm, the PASP2 data

TABLE 2
OPTICAL DEPTH AND COLUMN DENSITIES OF H_2O ICE

Object	τ[a]	FWHM[b] (cm^{-1})	$N(H_2O)$[c] (10^{18} cm^{-2})
IRAS 18511+0146	0.44 ± 0.04	460	1.0 ± 0.1
IRAS 21413+5442	0.73 ± 0.10	451	1.6 ± 0.1
IRAS 04579+4703	0.91 ± 0.08	404	1.8 ± 0.2

[a] Peak optical depth of H_2O ice absorption.
[b] Full width at half-maximum of H_2O ice absorption.
[c] Column density of H_2O ice calculated from the τ and FWHM.

by Ishii et al. (1998) were also used to estimate the continuum. The continuum for the 3.4 μm absorption was estimated by fitting a low-order polynomial function to the flux densities of the continuum points: second-order polynomials for IRAS 18511 and IRAS 21413 and a third-order polynomial for IRAS 04579 result in sufficient fits.[6] The derived continua are shown as dashed lines in Figure 2.The optical depths of the 3.4 μm feature are shown in Figure 3 as solid lines.

2.2. *Spectropolarimetry*

Spectropolarimetry from 3.09 to 3.71 μm of IRAS 18511 was carried out on the same night as the spectroscopic observations, using CGS4 and the spectropolarimetry module IRPOL2. CGS4 employed a 40 line mm^{-1} grating and a 2 pixel wide slit, resulting in the spectral resolution of 0.005 μm. Each pixel of the InSb array corresponds to 0.0025 μm, and the spectra were sampled with $\frac{1}{2}$ pixel shift. IRPOL2 combines a Wollaston prism and a rotatable half-wave plate to measure the linear polarization. One measurement consists of a set of four observations taken at half-wave plate angles of 0°, 45°, 22°.5, and 67°.5. For every position of the wave plate, the telescope was nodded about 10″. The total integration time was 32 minutes.

Reductions to each frame—bias subtraction, flat-fielding, background subtraction, and wavelength calibration—were performed in the same way as for the spectroscopic data (§ 2.1). Then, ordinary (o) and extraordinary (e) beams in each frame were extracted and combined for each angle of the wave plate. The ratios of o ray to e ray with the wave plate at 0° and 45° yield Stokes Q and the other two yield Stokes U:

$$q = \frac{Q}{I} = \frac{\sqrt{R_q} - 1}{\sqrt{R_q} + 1} , \quad u = \frac{U}{I} = \frac{\sqrt{R_u} - 1}{\sqrt{R_u} + 1} , \qquad (2)$$

where

$$R_q = \frac{[o/e]_0}{[o/e]_{45}} , \quad R_u = \frac{[o/e]_{22.5}}{[o/e]_{67.5}} . \qquad (3)$$

The resultant q and u spectra are shown in Figure 4*a*. In this and subsequent figures, data between 3.3 and 3.4 μm are omitted because the telluric methane absorptions near 3.3 μm and a deep absorption near 3.4 μm due to hydrocarbons in the optical cement of the Wollaston prism make the data useless (see Fig. 1 of Adamson et al. 1999). In Figure 4*a*, the spectra show a ripple and beating pattern. The phenomenon was also seen in the observations by Adamson et al. (1999), and they ascribe it to multiple reflections in the wave plates (see also Aitken & Hough 2001). Following Adamson et al. (1999), we performed a Fourier analysis to remove these artificial patterns. We found peaks at the frequency between 0.43 and 0.65 (Nyquist units)$^{-1}$ in the Fourier components. These components were set to zero before inverting the spectrum. The reconstituted q and u spectra are shown in Figure 4*b*, where the significant ripples are now absent. The degree of polarization $p(\lambda)$ and position angle θ were calculated from the q and u:

$$p = \sqrt{q^2 + u^2} , \quad \theta = 0.5 \arctan \frac{u}{q} . \qquad (4)$$

Instrumental polarization is estimated to be about 0.4% from the observations of an A5 V star, BS 7141, which is

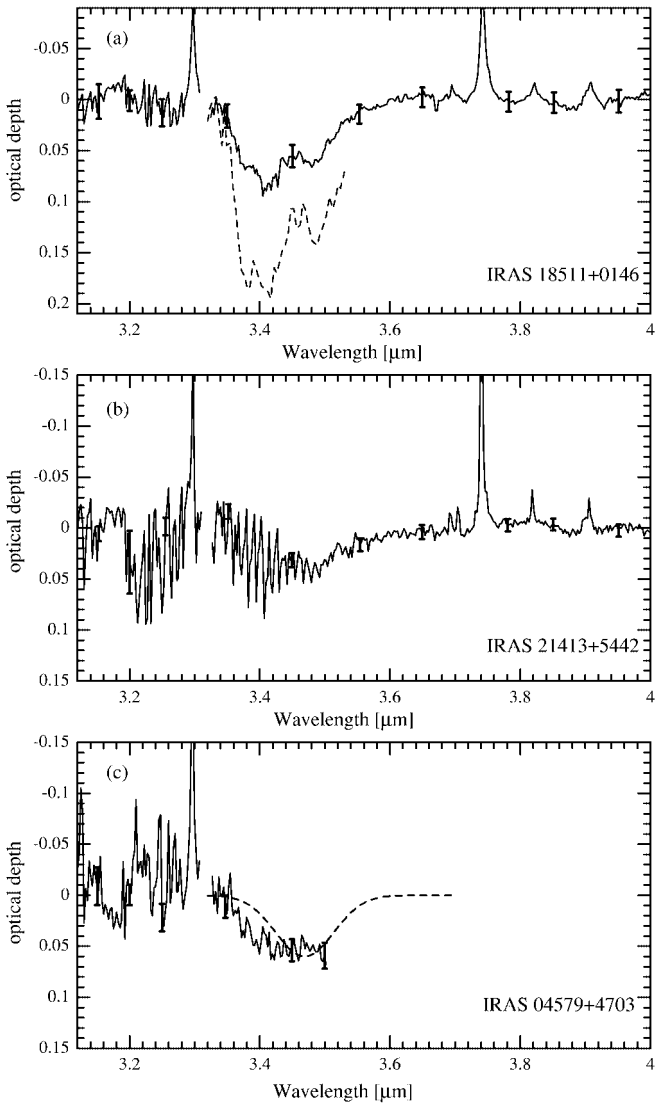

FIG. 3.—Optical depths relative to the continua indicated in Fig. 2. Some ± 1 σ error bars are indicated. The dashed line in (*a*) represents the 3.4 μm absorption observed in the line of sight to the Galactic center source IRS 7 by Sandford et al. (1991). The dashed line in (*c*) represents a Gaussian profile centered at 3.469 μm with FWHM of 0.105 μm, which is a typical profile of the 3.47 μm absorption in molecular clouds (Brooke et al. 1999).

[6] We also tried the fits to the logarithm of the flux densities as were done by Brooke et al. (1996, 1999). The resultant continua are almost the same as those from the fits to the flux densities.

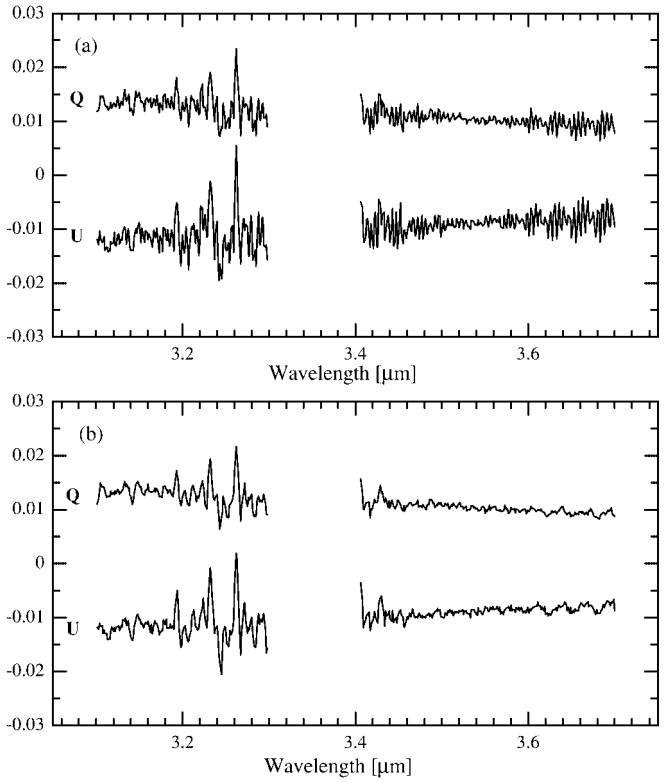

FIG. 4.—*Q* and *U* spectra of IRAS 18511 between 3.09 and 3.71 μm. Data between 3.3 and 3.4 μm are omitted because of the large noise. (*a*) Raw spectra and (*b*) spectra after removal of the wave-plate ripple are shown (see text).

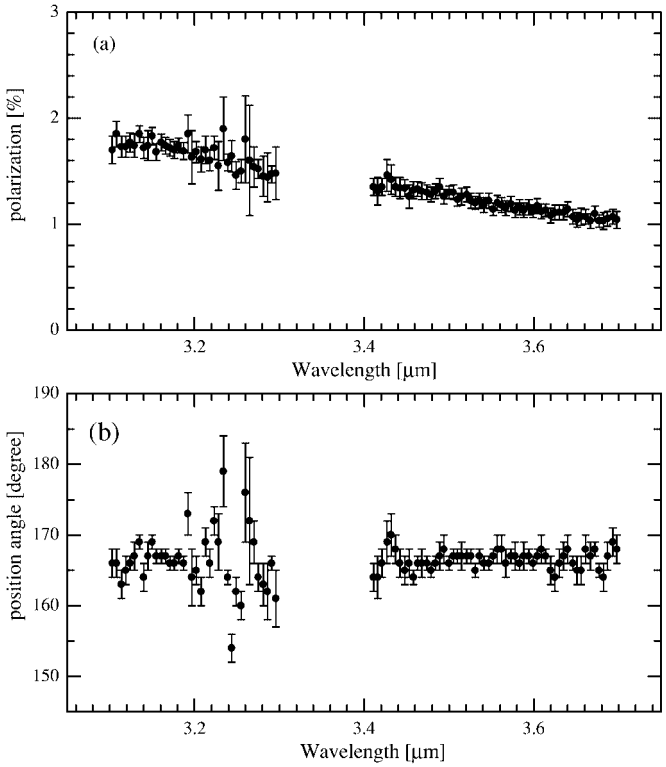

FIG. 5.—(*a*) Degree of polarization and (*b*) position angle of IRAS 18511, which were calculated from the *q* and *u* in Fig. 4*b*.

assumed to show no polarization. Calibrations for the polarization efficiency and the position angle were performed by following the CGS4/IRPOL manual on the UKIRT Web site.[7] The polarization efficiency ranges from 86% to 97% depending on the wavelength. A rotation of 7° was added to θ for the position angle calibration. Finally, the spectra were binned with an effective resolution of 0.005 μm. The results are shown in Figure 5.

3. DISCUSSION

3.1. *Absorption Profile of IRAS 18511*

Ishii et al. (1998) argued that the profile of the H_2O ice-band absorption between 2.8 and 3.8 μm for IRAS 18511 is similar to those observed previously in YSOs except for the presence of shallow absorptions at 3.4 μm on the long-wavelength wing of the ice absorption. In this section, we will describe the profiles of the H_2O ice absorption and the 3.4 μm absorption of this object.

The H_2O ice absorption in IRAS 18511 is characteristic of ice at a low temperature ($\lesssim$30 K; Fig. 3*a* of Smith et al. 1989) because the absorption shorter than 3.08 μm is significant (Fig. 2). However, the absorption width is larger than those observed in quiescent molecular clouds. This is shown in Figure 6, which compares the profile of IRAS 18511 (*solid line*) with that observed in the Taurus dark cloud in the line of sight to the background star Elias 16 (*dashed line*; Smith et al. 1989). The FWHM of H_2O absorption in IRAS 18511 (Table 2) is much broader than those of Elias 16 (345 ± 30 cm^{-1}; Teixeira & Emerson 1999) and other field stars behind the Taurus molecular cloud (Smith et al. 1993). On the other hand, the broad profile is similar to those found in luminous YSOs with circumstellar envelopes. As an example of ices in

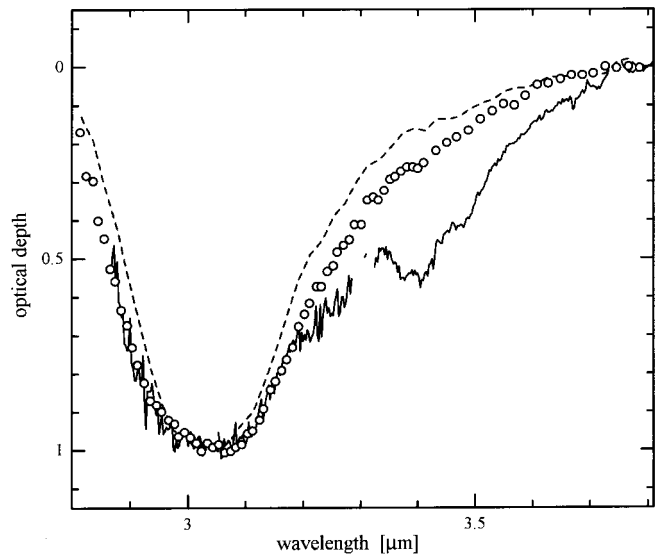

FIG. 6.—Optical depths of the 3 μm ice features of the Taurus cloud (Elias 16: *dashed line*; Smith et al. 1989) and of the YSO (S255 IRS 1: *open circles*; Smith et al. 1989) are compared with that of IRAS 18511 (*solid line*). For each source, the peak optical depth is scaled to 1. Spurious H I lines in IRAS 18511 are omitted for clarity.

[7] http://www.jach.hawaii.edu/JACpublic/UKIRT/instruments/irpol/CGS4/cgs4pol.html.

TABLE 3
OPTICAL DEPTHS AND COLUMN DENSITIES OF THE ALIPHATIC C–H FEATURES IN IRAS 18511+0146

Parameter	—CH_2— (Methylene)	—CH_3 (Methyl)
λ_0 (μm)	3.411	3.375
τ	0.087	0.066
$N(CH_2)$ (cm^{-2})	2.6×10^{17}	9.9×10^{16}

YSOs, we show the 3 μm feature of S255 IRS 1 in Figure 6 (*open circles*; Smith et al. 1989).

The 3.4 μm absorption in IRAS 18511 is easily distinguished from the long-wavelength wing of the H_2O ice absorption. The absorption, presented in Figure 3*a* as a solid line, shows the same profile as that observed in the DISM. For comparison, the 3.4 μm absorption of the Galactic center IRS 7 from Sandford et al. (1991) is also shown as a dashed line in Figure 3*a* as an example of the absorption in the DISM. The absorption profile in IRAS 18511 shows subfeatures at 3.38, 3.41, and 3.48 μm. The first and third features are characteristic, respectively, of the asymmetric and symmetric C–H stretching modes in the methyl group (—CH_3), and the second feature corresponds to the asymmetric C–H mode in the methylene group (—CH_2—). Following Pendleton et al. (1994), we calculated the column densities of —CH_2— and —CH_3 from the 3.41 and 3.38 μm features, respectively. The results are presented in Table 3. The ratio of methylene to methyl groups, $N(CH_2)/N(CH_3)$, is 2.6, which is similar to the ratios observed in the DISM (2–2.5; Pendleton et al. 1994).

The 3.47 μm absorption is known to correlate with the H_2O ice absorption (Brooke et al. 1999). We will examine if the absorption around 3.4 μm in IRAS 18511 shows the same correlation as the 3.47 μm absorption. In Figure 7, the optical depths of the 3.47 μm and H_2O ice absorption features from Brooke et al. (1999) are represented by open circles. The peak optical depth of the 3.41 μm absorption in IRAS 18511 is much larger than that expected from the correlation seen in molecular clouds, which is represented by a dashed line.

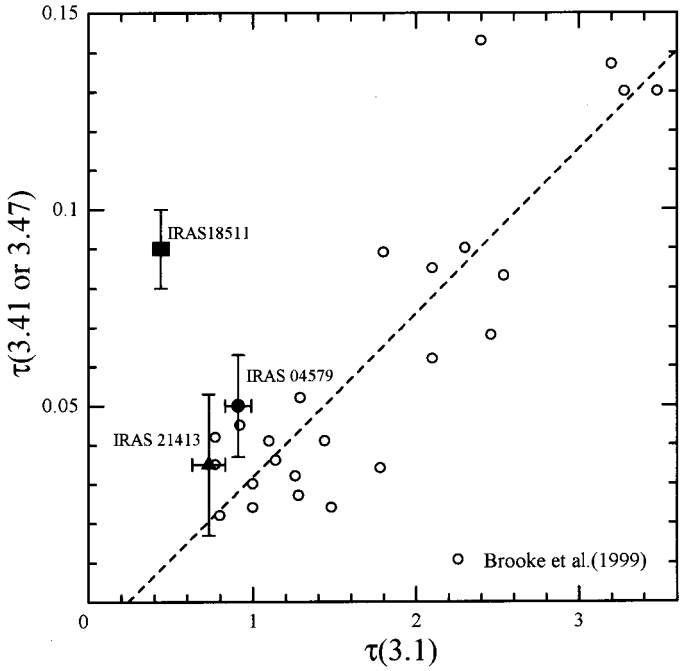

FIG. 7.—Optical depth of the 3.41 and 3.47 μm absorption is plotted against that of the H_2O ice absorption. Plots of $\tau_{3.41}$ for IRAS 18511, IRAS 21413, and IRAS 04579 are represented as a filled square, a filled triangle, and a filled circle, respectively. Open circles represent the plots of $\tau_{3.47}$ against the H_2O ice absorption taken from Brooke et al. (1999). The dashed line represents the relation between the 3.47 μm absorption and the 3.1 μm absorption, which is derived from the best (unweighted) linear fit to Brooke et al.'s data.

3.2. *Origin of the* 3.4 μm *Absorption in IRAS 18511*

As described above, the 3.4 μm feature in IRAS 18511 does not share any similarity with the 3.47 μm feature in molecular clouds in (1) the profile and (2) the relation to the H_2O ice absorption. Its profile is the same as those observed in the DISM that contains no H_2O ice. We will examine if the foreground DISM can plausibly cause the 3.4 μm feature in IRAS 18511.

The kinematic distance to IRAS 18511 is 3.9 kpc (Watt & Mundy 1999; Molinari et al. 1996). How much $\tau_{3.4}$ is expected over the DISM of this length? The 3.4 μm absorption is known to correlate with the amount of diffuse interstellar extinction, which is described by the relationship $A_{V,\mathrm{diff}}/\tau_{3.41} = 250 \pm 40$ mag (Pendleton et al. 1994). Application of this relationship to the optical depth measured for IRAS 18511 leads to an extinction $A_{V,\mathrm{diff}}$ of 22 ± 3 mag. If we adopt the average extinction value of the Galactic disk of 1.8 mag kpc^{-1} (Whittet 1992), then the $A_{V,\mathrm{diff}}$ will be only 7 mag. However, the extinction is highly patchy, and Cyg OB2 12 is known to have A_V of 10.2 ± 0.3 mag at a distance of 1.7 ± 0.2 kpc (references in Whittet et al. 1997). Thus, the $A_{V,\mathrm{diff}}$ of 22 mag for IRAS 18511 can be explained if the sight line to the object suffers a similar amount of extinction per distance as in the sight line to Cyg OB2 12.

If we correct the observed K magnitude of 6.6 mag of IRAS 18511 for the $A_{V,\mathrm{diff}}$ of 22 mag, assuming the interstellar reddening law by Rieke & Lebofsky (1985), and consider the distance of 3.9 kpc, then its absolute magnitude at K becomes $M_K = -8.8$ mag, which is one of the brightest among the massive YSOs (Chan, Henning, & Schreyer 1996). IRAS 18511[8] is located at the northwestern edge of the $C^{18}O$ $J = 1$–0 emission, which has an extent of roughly $41'' \times 24''$ (Watt & Mundy 1999). At the peak of the $C^{18}O$ emission, a compact radio source was detected about $20''$ southeast from IRAS 18511.[9] Molinari et al. (2000) derived the H_2 column density of 6.2×10^{22} cm^{-2} (corresponding to $A_V = 65$ mag) for the region from submillimeter continuum observations. Thus, IRAS 18511 is associated with a massive star-forming region that contains at least another early-type star.

After the interstellar reddening correction using the above $A_{V,\mathrm{diff}}$ value, the observed $H-K$ color of 2.8 mag is corrected to 1.4 mag, and the $K-L$ color of 2.6 mag becomes 1.4 mag (Campbell, Persson, & Matthews 1989;

[8] The NIR position is $\alpha = 18^h53^m37^s.88$, $\delta = +1°50'30''.8$ (J2000) (Ishii et al. 2002), which is consistent with that of the object 06′ of Campbell, Persson, & Matthews (1989).

[9] There is no bright NIR source at the position of the compact H II region, but faint and red sources were found (Ishii et al. 2002). Also a slight elongation of the bright source to the southeast is seen in the MSX map at 8 μm (http://irsa.ipac.caltech.edu/docs).

Ishii et al. 1998). These remaining color excesses are probably due to absorption by dust in the molecular cloud and also to the circumstellar emission. The extinction due to the molecular cloud $A_{V,\mathrm{mol}}$ can be estimated from the column density of H_2O ice (Table 2), although the relationship between them should vary from cloud to cloud (Smith et al. 1993; Tanaka et al. 1990). For IRAS 18511, $A_{V,\mathrm{mol}}$ is estimated to be 12 ± 2 or 22 ± 2, where the former and the latter are derived by using the relationship in the Taurus and Ophiuchus clouds, respectively (Teixeira & Emerson 1999). The $A_{V,\mathrm{mol}}$ is smaller than that derived from the H_2 column density of the molecular cloud (Molinari et al. 2000), suggesting that IRAS 18511 is embedded in the cloud.

We can determine the silicate absorption for IRAS 18511 from the IRAS Low Resolution Spectrometer data (Volk et al. 1991).[10] The data show a very strong silicate absorption around 10 μm and a weaker absorption at $\sim$17 μm. The optical depth of the absorption feature at $\sim$17 μm is about 1. The signals around 10 μm are negative, but if we assume $\tau_{18}/\tau_{9.7} \sim 0.4$ (Pegourie & Papoular 1985; Simpson 1991), then $\tau_{9.7}$ is $\sim$2.5. We note that the ratio $\tau_{3.41}/\tau_{9.7}$ for IRAS 18511 is $\sim$0.035 and is smaller than the ratio $\sim$0.079 for Cyg OB2 12 (Sandford et al. 1995). This is a natural consequence if the 3.4 μm absorbers are present only in the DISM and the silicate absorption occurs both in the DISM and in the molecular cloud in the line of sight to IRAS 18511.

From the above, we conclude that although IRAS 18511 has both the H_2O ice and the 3.4 μm absorption, they are probably produced in different regions. Therefore, the —CH_2— and —CH_3 bands at 3.4 μm have not yet been detected in molecular clouds. If the lifetime of a carbonaceous dust grain is $\sim 4 \times 10^8$ yr (Jones et al. 1994) and it cycles back and forth between molecular clouds and the DISM, there must be some mechanism to make the 3.4 μm hydrocarbon bands undetectable in molecular clouds.

[10] Although we checked the *ISO* archive, we found no data from which one could estimate the depth of the silicate feature.

3.3. *IRAS 04579 and IRAS 21413*

The H_2O ice absorption in IRAS 04579 and IRAS 21413 is similar to that of YSOs in that the absorption width is larger than that found in a quiescent molecular cloud. In Figure 8, we compare the profiles of our objects with those of YSOs with similar absorption peaks and widths; the YSO data are taken from Smith et al. (1989). The profile of IRAS 21413 is similar to that of GL 2591, including the long-wavelength wing. For the comparison with IRAS 04579, we selected S255 IRS 1 because its absorption wing is largest among the group fitted by low-temperature ices (23 K, from Smith et al.'s model). While the absorptions shortward of 3.3 μm resemble each other, the longer wavelength absorption is larger in IRAS 04579 than in S255 IRS 1.

As shown in Figure 8*a*, the long-wavelength wing absorption in IRAS 21413 is similar to that of previously studied YSOs, contrary to the result of the low-resolution spectroscopy by Ishii et al. (1998). Thus, it is likely that IRAS 21413 shows little or no 3.4 μm absorption from the DISM. Unfortunately, we cannot derive any conclusion from the absorption profile itself (Fig. 3*b*), because the poor cancellation of the telluric methane absorptions in the 3.2–3.5 μm region prevents us from looking for any structures in the optical depth profile.

We were not able to cover the whole range of the 3 μm absorption in IRAS 04579. However, the 3.4 μm dip in this object seems to be different from those in the long-wavelength wings observed in YSOs. The 3.4 μm absorption, presented in Figure 3*c* as a solid line, is broader than the 3.47 μm absorption in molecular clouds. The central wavelength and width of the 3.47 μm feature in molecular clouds are $\lambda_0 = 3.469 \pm 0.002$ μm and FWHM $= 0.105 \pm 0.004$ μm (Brooke et al. 1999). For comparison, we plot the typical profile of the 3.47 μm feature in Figure 3*c* as a dashed line. The figure shows that the absorption shortward of $\sim$3.4 μm in IRAS 04579 is deeper than that expected from the profile of the molecular cloud feature at 3.47 μm. This does not depend on the wavelength range we adopted as the continuum (§ 2.1): even if we use the continuum defined for the

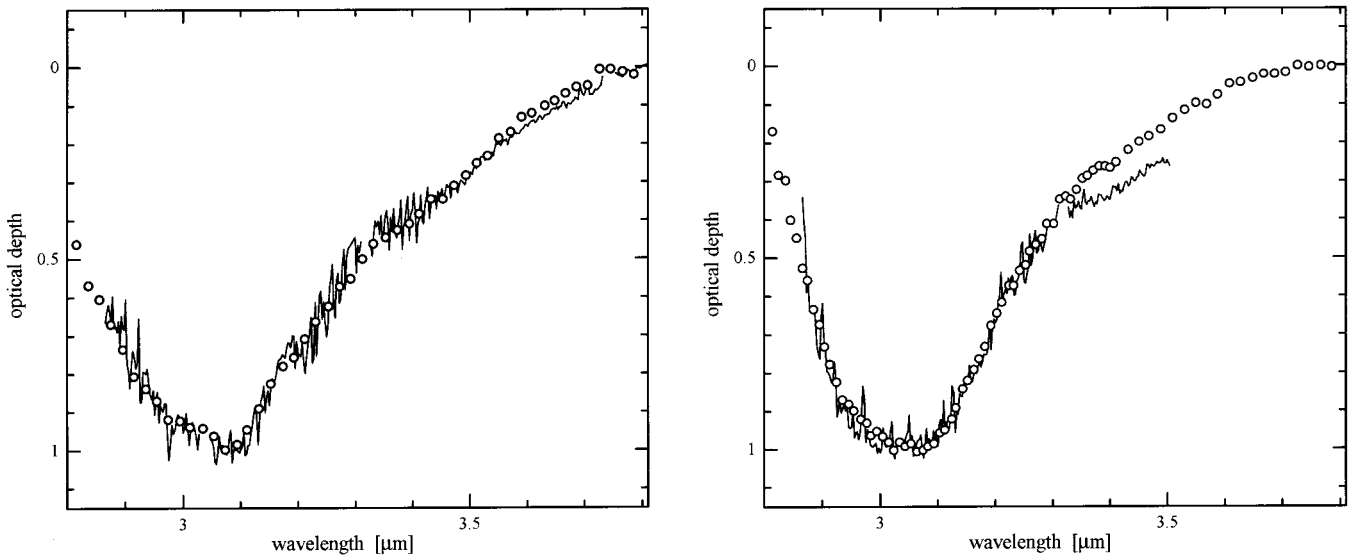

FIG. 8.—(*a*) Optical depths of the 3 μm ice features of IRAS 21413 (*solid line*) is compared with that of GL 2591 (*open circles*; Smith et al. 1989). (*b*) Optical depths of the 3 μm ice features of IRAS 04579 (*solid line*) is compared with that of S255 IRS 1 (*open circles*; Smith et al. 1989). For each source, the peak optical depth is scaled to 1. Spurious H I lines in IRAS 21413 and IRAS 04579 are omitted for clarity.

3.47 μm absorption by Brooke et al. (1999), the absorption profile in IRAS 04579 changes little. On the other hand, we found no substructure in the 3.4 μm absorption for IRAS 04579, which is unlike the DISM feature. In Figure 7, the 3.4 μm to H_2O absorption ratio of this object is in the range of other YSOs but somewhat larger. Therefore, it is likely that there is small contribution from the foreground 3.4 μm feature in the DISM, superposed on the 3.47 μm absorption in the molecular cloud. The large distance to the object (2.5–2.7 kpc; Molinari et al. 1996; Wouterloot & Brand 1989) also supports this view.

3.4. *Polarimetric Behavior of the* 3 μm *Absorptions*

Interstellar polarization is well represented by a power law $p(\lambda) \propto \lambda^{-\beta}$, with $\beta \sim 1.6$–2 (Nagata 1990; Martin et al. 1992). Polarization of IRAS 18511 (Fig. 5) shows a steeper wavelength dependence with $\beta \sim 3.2$. We believe that this is due to the 3 μm absorption feature. Therefore, we estimate the excess polarization Δp by defining the continuum polarization with $\beta = 1.8$ to pass through the data at around 3.7 μm. Since the position angle is nearly constant over the observed wavelength range, the continuum component and the excess component seem to have similar position angles. The continuum is shown in Figure 9*a* as a dashed line, and the excess polarization Δp, derived by subtracting the continuum polarization from the observed one, is shown in Figure 9*b* as filled circles.

The excess polarization in Figure 9*b* shows a profile similar to that of the 3 μm absorption, which is represented by solid lines. The ratio of Δp to the ice absorption, $\Delta p/\tau$, is about 1%, which is within the range observed for the H_2O ice feature (Hough et al. 1989). Thus, the excess polarization is most likely due to the ice absorption. The icy grains seem to be aligned in similar position angles to the grains that cause the continuum polarization.

Next we will examine if the 3.4 μm absorption is accompanied by a polarization excess. The continuum polarization for the 3.4 μm feature is defined in the same way as for the extinction feature: it is derived by fitting a second-order polynomial to the points at 3.13–3.18 and 3.61–3.71 μm. The continuum is shown in Figure 9*a* as a solid line. The excess polarization over the continuum $\Delta p_{3.4}$ is shown in Figure 9*c* by filled circles along with the optical depth of the 3.4 μm feature (*solid line*). Figure 9*c* shows that there is no excess polarization at around 3.4 μm, and the upper limit is $\Delta p/\Delta\tau_{3.41} < 1\%$.

The polarimetric behavior of the 3.4 μm absorption in IRAS 18511 differs from that of the 3.47 μm absorption in molecular clouds where excess polarization was observed with the ratio $\Delta p/\Delta\tau_{3.47} \sim 10\%$ in the spectrum of the BN object (Hough et al. 1996).

This indicates that the grains responsible for the 3.4 μm feature are not aligned or they are optically isotropic. Thus, the carrier of the 3.4 μm feature does not coexist with the H_2O ice, which is thought to be present as mantles on the elongated silicate core; this is consistent with the discussion in § 3.2. Moreover, although the carrier is likely to be located in the DISM, it is physically separated from other polarizing grains in the DISM because at least some of the continuum polarization following the power law must be produced by them. The result of our observation is consistent with the 3.4 μm feature in GC IRS 7, where no excess polarization was found with an upper limit $\Delta p/\Delta\tau_{3.4} < 0.2\%$ (Adamson et al. 1999).

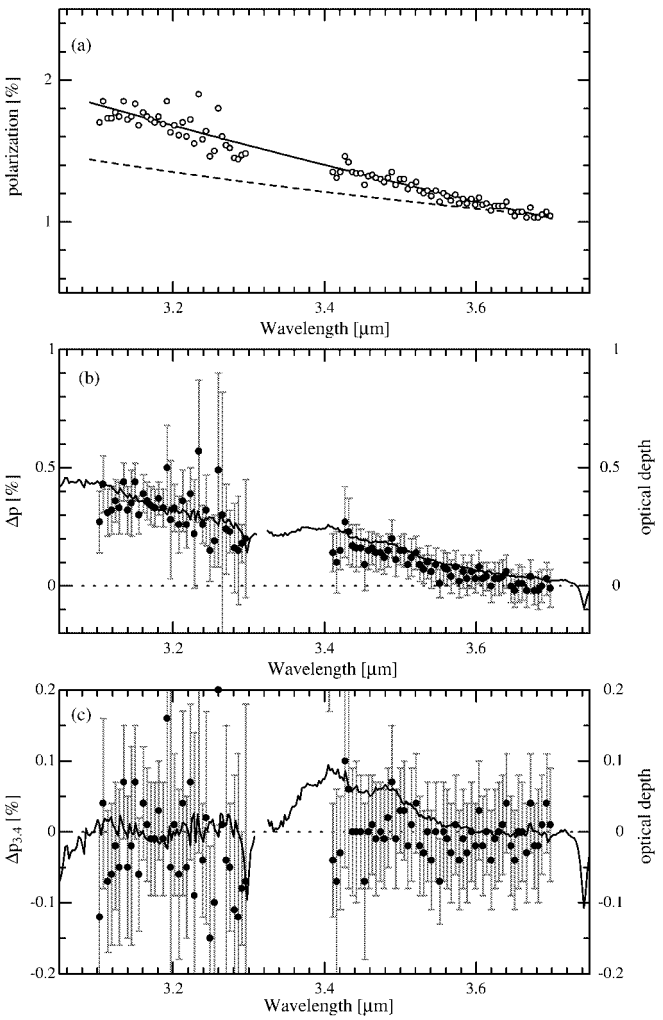

FIG. 9.—Excess polarization for the 3 μm features. (*a*) Open circles represent the polarization of IRAS 18511, which are same as those shown in Fig. 5 but error bars are omitted for clarity. The dashed line is the assumed interstellar polarization (see text). The solid line represents the continuum for the 3.4 μm absorption, which is derived by fitting a second-order polynomial to the points at 3.13–3.18 and 3.61–3.71 μm. (*b*) Excess above the interstellar polarization is represented by filled circles. The solid line represents the optical depths of the 3 μm absorptions, which is the same as shown in Fig. 2*a*. (*c*) Filled circles represent the residual polarization after subtracting the continuum for the 3.4 μm feature (Fig. 9*a*, *solid line*). The solid line represents the optical depths of the 3.4 μm absorptions, which is the same as shown in Fig. 3*a*.

4. CONCLUSIONS

Spectroscopy of the 3 μm band in three YSOs—IRAS 18511, IRAS 04579, and IRAS 21413—was made to investigate the 3.4 μm absorption on the shoulder of the long-wavelength wing of the H_2O ice absorption. Spectropolarimetry of the 3.4 μm absorption was also performed for IRAS 18511. The main results are the following:

1. The 3.4 μm absorption in IRAS 18511 is clearly different from the 3.47 μm feature in molecular clouds in the profile and in the relation to the 3 μm H_2O ice absorption. The profile of the 3.4 μm feature is the same as that observed

in the DISM, leading us to attribute the origin of the feature to the foreground DISM. IRAS 18511 must suffer A_V of $\sim$22 mag in the DISM.

2. We found no excess polarization accompanying the 3.4 μm feature in IRAS 18511. This agrees with previous observations toward the Galactic center source IRS 7 by Adamson et al. (1999) and supports the idea that the carrier resides in a population of small, nonpolarizing carbonaceous grains, which is physically separate from other polarizing grains.

3. For IRAS 04579 and IRAS 21413, it is not clear whether the 3.4 μm absorptions have a similar profile to that in diffuse clouds or in molecular clouds. Because the whole 3 μm profile of IRAS 21413 resembles that of a molecular cloud source, we infer that there is little or no 3.4 μm absorption like that seen in the DISM. For IRAS 04579, it is possible that part of the 3.4 μm absorptions occurs in the foreground DISM, because (1) the width is wider than that of the 3.47 μm feature in molecular clouds and (2) the distance to the object is large enough that extinction in the DISM might be enough to contribute to the 3.4 μm feature.

We would like to thank the staff at the Joint Astronomy Centre and UKIRT for providing the support to carry out the observations. The United Kingdom Infrared Telescope is operated by the Joint Astronomy Centre on behalf of the UK Particle Physics and Astronomy Research Council. We thank the Department of Physical Sciences, University of Hertfordshire, for providing IRPOL2 for the UKIRT.

REFERENCES

Adamson, A. J., Whittet, D. C. B., Chrysostomou, A., Hough, J. H., Aitken, D. K., Wright, G. S., & Roche, P. F. 1999, ApJ, 512, 224
Aitken, D. K., & Hough, J. H. 2001, PASP, 113, 1300
Allamandola, L. J., Sandford, S. A., & Tielens, A. G. G. M. 1992, ApJ, 399, 134
———. 1993, Science, 264, 64
Brooke, T. Y., Sellgren, K., & Geballe, T. R. 1999, ApJ, 517, 883
Brooke, T. Y., Sellgren, K., & Smith, R. G. 1996, ApJ, 459, 209
Campbell, B., Persson, S. E., & Matthews, K. 1989, AJ, 98, 643
Chan, S. J., Henning, T., & Schreyer, K. 1996, A&AS, 115, 285
d'Hendecourt, L. B., & Allamandola, L. J. 1986, A&AS, 64, 453
Gezari, D. Y., Schmitz, M., Pitts, P. S., & Mead, J. M. 1993, Catalog of Infrared Observations (NASA RP-1294, 3d ed.; Washington: NASA)
Hough, J. H., Chrysostomou, A., Messinger, D. W., Whittet, D. C. B., Aitken, D. K., & Roche, P. F. 1996, ApJ, 461, 902
Hough, J. H., Whittet, D. C. B., Sato, S., Yamashita, T., Tamura, M., Nagata, T., Aitken, D. K., & Roche, P. F. 1989, MNRAS, 241, 71
Imanishi, M., Sasaki, Y., Goto, M., Kobayashi, N., Nagata, T., & Jones, T. J. 1996, AJ, 112, 235
Ishii, M., Hirao, T., Nagashima, C., Nagata, T., Sato, S., & Yao, Y. 2002, AJ, 124, 430
Ishii, M., Nagata, T., Sato, S., Watanabe, M., Yao, Y., & Jones, T. J. 1998, AJ, 116, 868
Ishii, M., Nagata, T., Sato, S., Yao, Y., Jiang, Z., & Nakaya, H. 2001, AJ, 121, 3191
Jones, A. P., Tielens, A. G. G. M., Hollenbach, D. J., & McKee, C. F. 1994, ApJ, 433, 797
Martin, P. G., et al. 1992, ApJ, 392, 691
Molinari, S., Brand, J., Cesaroni, R., & Palla, F. 1996, A&A, 308, 573
Molinari, S., Brand, J., Cesaroni, R., & Palla, F. 2000, A&A, 355, 617
Nagata, T. 1990, ApJ, 348, L13
Pegourie, B., & Papoular, R. 1985, A&A, 142, 451
Pendleton, Y. J., Sandford, S. A., Allamandola, L. J., Tielens, A. G. G. M., & Sellgren, K. 1994, ApJ, 437, 683
Rieke, G. H., & Lebofsky, M. J. 1985, ApJ, 288, 618
Sandford, S. A., Allamandola, L. J., Tielens, A. G. G. M., Sellgren, K., Tapia, M., & Pendleton, Y. 1991, ApJ, 371, 607
Sandford, S. A., Pendleton, Y., & Allamandola, L. J. 1995, ApJ, 440, 697
Sellgren, K., Smith, R. G., & Brooke, T. Y. 1994, ApJ, 433, 179
Simpson, J. P. 1991, ApJ, 368, 570
Smith, R. G., Sellgren, K., & Brooke, T. Y. 1993, MNRAS, 263, 749
Smith, R. G., Sellgren, K., & Tokunaga, A. T. 1989, ApJ, 344, 413
Soifer, B. T., Russell, R. W., & Merrill, K. M. 1976, ApJ, 207, L83
Tanaka, M., Sato, S., Nagata, T., & Yamamoto, T. 1990, ApJ, 352, 724
Teixeira, T. C., & Emerson, J. P. 1999, A&A, 351, 292
Tielens, A. G. G. M., Wooden, D. H., Allamandola, L. J., Bregman, J., & Witteborn, F. C. 1996, ApJ, 461, 210
Tokunaga, A. T. 2000, in Astrophysical Quantities, ed. A. N. Cox (4th ed.; New York: AIP), 143
Volk, K., Kwok, S., Stencel, R. E., & Brugel, E. 1991, ApJS, 77, 607
Watt, S., & Mundy, L. G. 1999, ApJS, 125, 143
Whittet, D. C. B. 1992, Dust in the Galactic Environment (Bristol: Inst. Phys.)
Whittet, D. C. B., Boogert, A. C. A., Gerakines, P. A., Schutte, W., Tielens, A. G. G. M., de Graauw, T., Prusti, T., & van Dishoeck, E. F. 1997, ApJ, 490, 729
Wouterloot, J. G. A., & Brand, J. 1989, A&AS, 80, 149